Politecnico di Torino
Master Degree in Physics of Complex Systems

Inhomogeneous asymmetric exclusion processes: steady-state and relaxation transitions

Academic year: 2023/2024

Supervisors: Alessandro Pelizzola, Marco Pretti

Candidate: Lorenzo Avertano

Contents

List of Abbreviations

TASEP: Totally Asymmetric Simple Exclusion Process
MFT: Mean Field Theory
PA: Pair Approximation
MCS: Monte Carlo simulation
DWT: Domain Wall Theory
DW: Domain Wall
DDW: Delocalized domain wall
OBC: Open boundary conditions
FP: Fokker-Planck
LD: Low density
HD: High density
MC: Maximal current

1 Introduction

The Asymmetric Exclusion Process represents a fundamental family of models in out of equilibrium statistical physics, for which applications are found in a large variety of contexts, ranging from biology (e.g. the motion of ribosomes along mRNA or molecular motors on intracellular filaments) to electron hopping transport with applied voltage and vehicular highway traffic.

The specific model we want to consider for this work is the Totally Asymmetric Simple Exclusion Process (TASEP) [1]. It is defined on a one dimensional lattice, where particles can hop only rightward, from each node to the next one, provided the latter is empty. Despite its simplicity, it can offer a very interesting series of results, depending on the characteristics with which we equip it. We work with open boundary conditions (OBC) and inhomogeneous hopping rates (smoothly varying). Indeed, in real life we expect to find conditions that alter the ideal condition of uniform rate. The most interesting aspect is that in this regime all the steady-state transitions are first order, as shown in [2]. In this regime, a good agreement between the Mean Field Theory (MFT) and numerical simulations has been found [2, 3].

The purpose of this work is not tied to a specific application of this model, but rather to a theoretical exploration; in particular, we aim to find: the steady-state transitions both analytically, using Fokker-Planck (FP) equation, and numerically, using Monte Carlo simulations (MCS); the relaxation transitions in MFT and Pair Approximation (PA); the Domain Wall Theory (DWT) picture; the full master equation picture.
This thesis is organised as follows. In Section 2 we define the model. In Section 3 we discuss the theoretical methods we used and the Gillespie Algorithm. Then, in Section 4 we present the results of the work and final considerations can be found in Section 5.

2 Models

The model is defined on a one-dimensional lattice of L sites, that are labeled by variable i from 1 to L. For the occupation of the i-th site we define the variable n_i^t, that assumes value 1 if the site is occupied at time t and 0 if it is empty. For the average occupation we define the local density $\rho_i^t = \langle n_i^t \rangle$. In this case $\langle ... \rangle$ means temporal average.
For the terminal sites one can consider periodic or OBC. We choose to work with the second one.
The hopping rate for the jump from site i to site i+1 is q_i. We will consider the inhomogeneous case where hopping rates are different, but smoothly varying (cosinusoidal behavior).
Is is important to state that in this system the particle-hole symmetry applies, where an hole is an empty site (Fig. 1). This symmetry implies that the properties of the system in the High Density (HD) phase are equivalent to those in the high hole density phase, and vice versa. It means that there is no need to study both the HD and Low Density (LD) phases separately, and it is particularly important for the transition to the Maximal Current (MC) phase. Details on the different phases will follow.

2.1 Master equation and transition rate matrix

For the evolution of the system we can introduce the master equation of the process, that takes into account the probabilities of the 2^L possible states. Denoting by $n = (n_1, ..., n_L)$ a configuration and by $P^t(n)$ the probability of being in configuration n at time t, the master equation is:

$$\dot{P}^t(n) = \sum_m W_{n,m} P^t(m), \tag{1}$$

where $W_{n,m}$ are the elements of the transition rate matrix. Introducing $\mathscr{W}(m \to n)$ as the transition rate from configuration m to n:

$$\begin{aligned} W_{n,m} &= \mathscr{W}(m \to n) - \delta_{n,m} \sum_l \mathscr{W}(n \to l) \\ &= \begin{cases} \mathscr{W}(m \to n), & \text{if } m \neq n \\ -\sum_{l \neq n} \mathscr{W}(n \to l), & \text{if } m = n \end{cases}. \end{aligned} \tag{2}$$

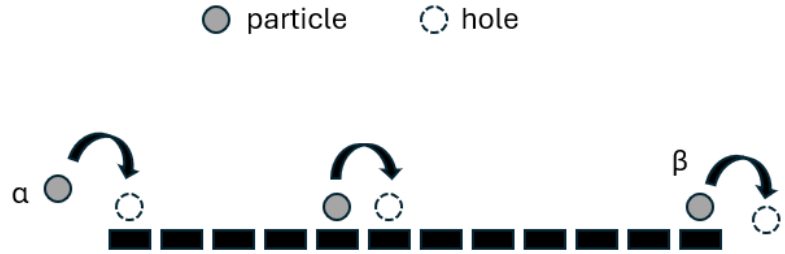

Figure 1: TASEP with OBC.

2.2 TASEP with open boundary conditions

Considering OBC, particles are injected at the leftmost node, provided it is empty, with rate α, and extracted from the rightmost node, provided it is occupied, with rate β (Fig. 1). An equivalent description can be obtained assuming that the system is in contact with two reservoirs of fixed densities $\rho_l = \alpha$ and $\rho_r = 1 - \beta$.

In order to obtain the master equation for TASEP with OBC we observe that transitions between different configurations can occur because of $L + 1$ possible processes, namely injection at node 1, hopping from node k to node $k + 1$ ($k = 1, ..., L - 1$) and extraction from node L. Once the master equation is obtained, we can try to solve it but its size (2^L) is too large for a direct approach, so we can consider the evolution of the single-node marginals. After the calculations [4] we are left with:

$$\dot{\rho_i^t} = \dot{P_i^t}(1) = J_{i-1}^t - J_i^t, \qquad i = 1, ..., L, \tag{3}$$

so the evolution of the local densities is described by a continuity equation, where:

$$\begin{aligned} J_i^t &= q_i P_i^t(1,0), \qquad i = 1, ..., L-1, \\ J_0^t &= \alpha(1 - \rho_1^t), \\ J_L^t &= \beta \rho_L^t. \end{aligned} \tag{4}$$

2.3 Phase diagram and phase boundaries

After introducing the model, we can now delve into its stationary phases in MFT. Following [2], we take the thermodynamic limit (sites are labeled by $x = i/L$ with $L \to \infty$) and for the bulk current we get:

$$J = q(x)\rho(x)[1 - \rho(x)], \tag{5}$$

where $\rho(x) = \langle n_i \rangle$ is the steady-state density at x. In the steady-state the current J must be constant. For the hopping rate function $q(x)$ it is convenient (calculation reasons) to define the function:

$$\tau(x) = \frac{1}{q(x)} = -\frac{\tau_{max} - 1}{2}\cos(2\pi x) + \frac{\tau_{max} + 1}{2}, \tag{6}$$

where τ_{max} is the maximum of $\tau(x)$ and the smoothly varying function $q(x)$ can be seen in Fig. 2 for $\tau_{max} = 2$. This value of τ_{max} will be adopted in the next steps and Sections.

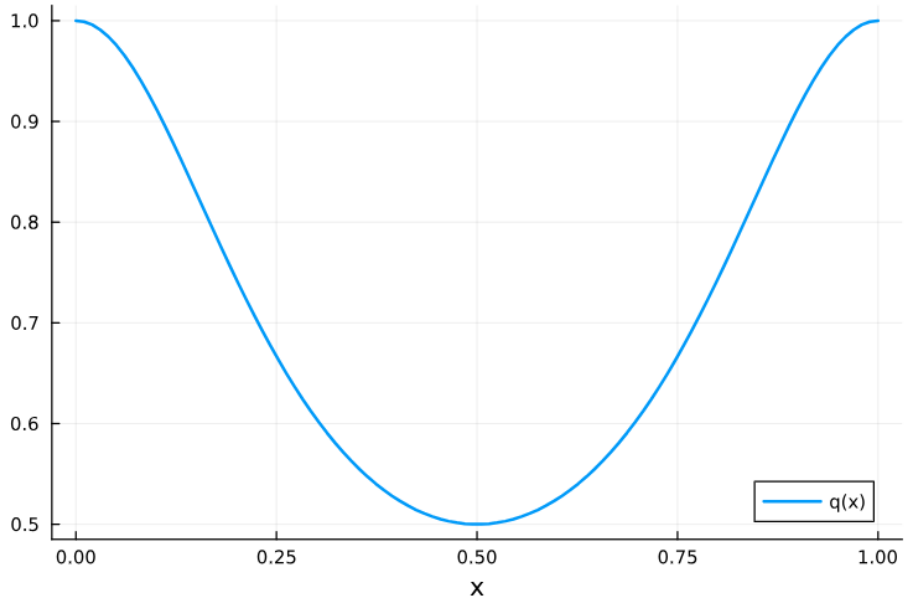

Figure 2: Hopping rate function $q(x)$.

Equation (5) has two nonuniform solutions $\rho_+(x)$ and $\rho_-(x)$:

$$\rho_+(x) = \frac{1}{2}\left[1 + \sqrt{1 - 4J\tau(x)}\right] > \frac{1}{2}, \tag{7}$$

$$\rho_-(x) = \frac{1}{2}\left[1 - \sqrt{1 - 4J\tau(x)}\right] < \frac{1}{2}. \tag{8}$$

Since the density function $\rho(x)$ must be real, we get the condition on J:

$$J \leq \frac{1}{4\tau(x)}, \tag{9}$$

that must hold for all x. As a consequence $J_{max} = \frac{1}{4\tau_{max}}$.

LD phase. For the investigation of the LD phase, we start noticing that the injection (with rate α) and the extraction (with rate β) are equivalent to adding two sites at the boundaries, that are constantly set to the density α and $1-\beta$ respectively [5]. Since we are considering an infinite number of sites, we can state that $\rho(0) = \alpha$, and we get:

$$J_{LD} = \frac{1}{\tau(0)}\alpha(1-\alpha). \tag{10}$$

We have to notice that $J_{LD} < \frac{1}{4\tau_0}$ [2], and due to (5) the steady-state bulk density in this phase must be smaller that $1/2$ everywhere. Then, the density profile is given by:

$$\rho_{LD}(x) = \frac{1}{2}\left[1 - \sqrt{1 - 4\frac{\tau(x)}{\tau(0)}\alpha(1-\alpha)}\right] < \frac{1}{2}. \tag{11}$$

The result is shown in Fig. 3.

HD phase. Following the same logic, since $\rho(1) = 1-\beta$, the current is:

$$J_{HD} = \frac{1}{\tau(1)}\beta(1-\beta), \tag{12}$$

and the density profile is:

$$\rho_{HD}(x) = \frac{1}{2}\left[1 + \sqrt{1 - 4\frac{\tau(x)}{\tau(1)}\beta(1-\beta)}\right] > \frac{1}{2}. \tag{13}$$

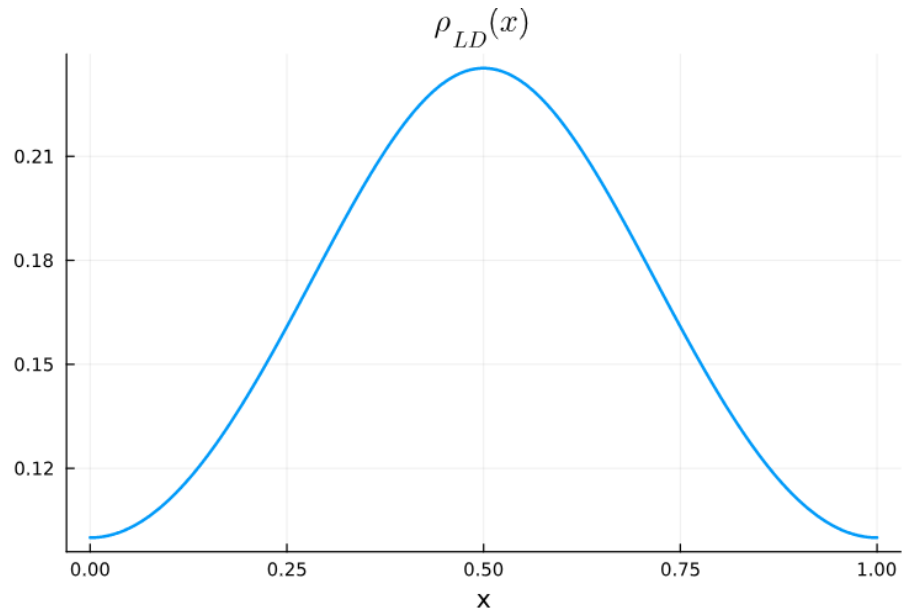

Figure 3: LD phase in MFT for $\alpha = 0.1$.

The result is shown in Fig. 4.

MC phase. Within this phase the current reaches its maximum:

$$J_{MC} = \frac{1}{4\tau_{max}}, \tag{14}$$

that can be used both in $\rho_-(x)$ and $\rho_+(x)$, with these profiles becoming identical (and equal to 1/2) at x_0, for which $\tau(x_0) = \tau_{max}$; but the density profile is not easy to obtain. Considering an heuristic argument as done in [2], one can show that:

$$\rho(x) = \begin{cases} \rho_+(x), & \text{if } 0 \leq x \leq x_0 \\ \rho_-(x), & \text{if } x_0 < x \leq 1 \end{cases}. \tag{15}$$

The result is shown in Fig. 5.

Phase boundaries. We start considering the boundary between LD and HD phases. The condition is given by $J_{LD} = J_{HD}$:

$$\frac{1}{\tau(0)}\alpha(1-\alpha) = \frac{1}{\tau(1)}\beta(1-\beta), \tag{16}$$

and, since $\tau(0) = \tau(1)$, the phase boundary is dictated by $\alpha = \beta$.

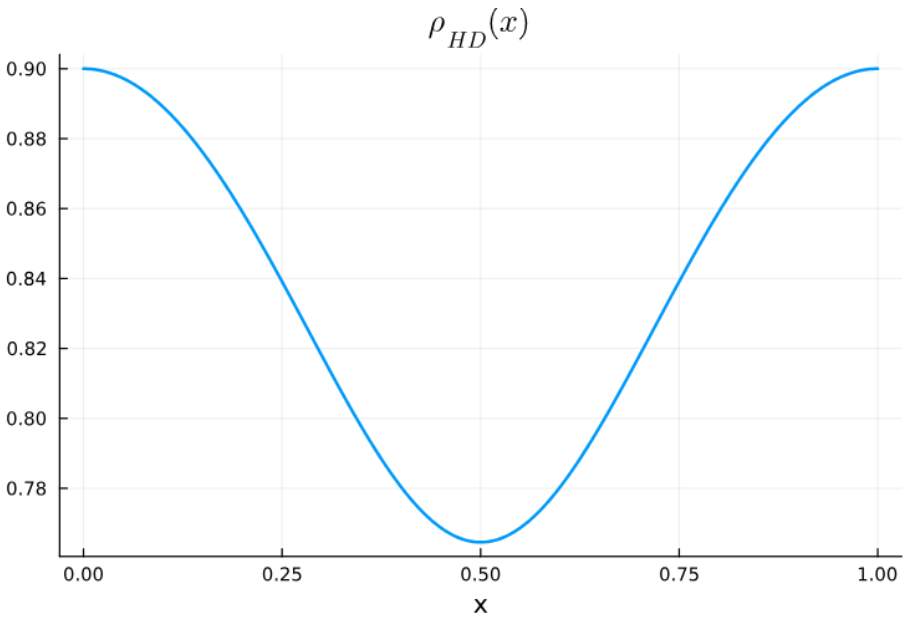

Figure 4: HD phase in MFT for $\beta = 0.1$.

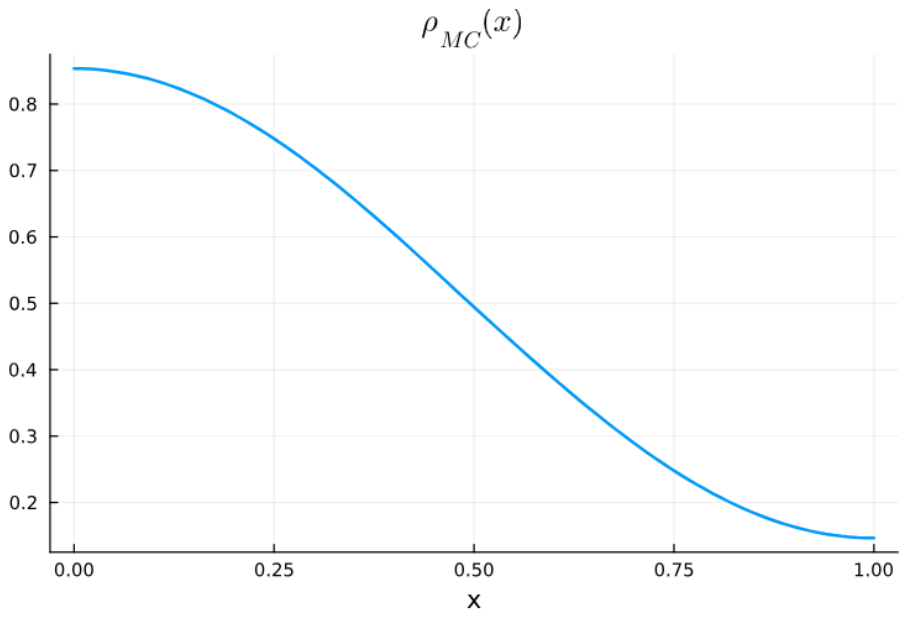

Figure 5: MC phase in MFT.

For the LD-MC boundary, the condition $J_{LD} = J_{MC}$ gives:

$$\alpha = \frac{1}{2}\left[1 - \sqrt{1 - \frac{\tau(0)}{\tau_{max}}}\right] \doteq \mathscr{T} \tag{17}$$

For the HD-MC boundary, the condition $J_{HD} = J_{MC}$ gives:

$$\beta = \mathscr{T} \tag{18}$$

The phase diagram can be seen in Fig. 6. The three phase boundaries meet at $\left(\mathscr{T}, \mathscr{T}\right)$.

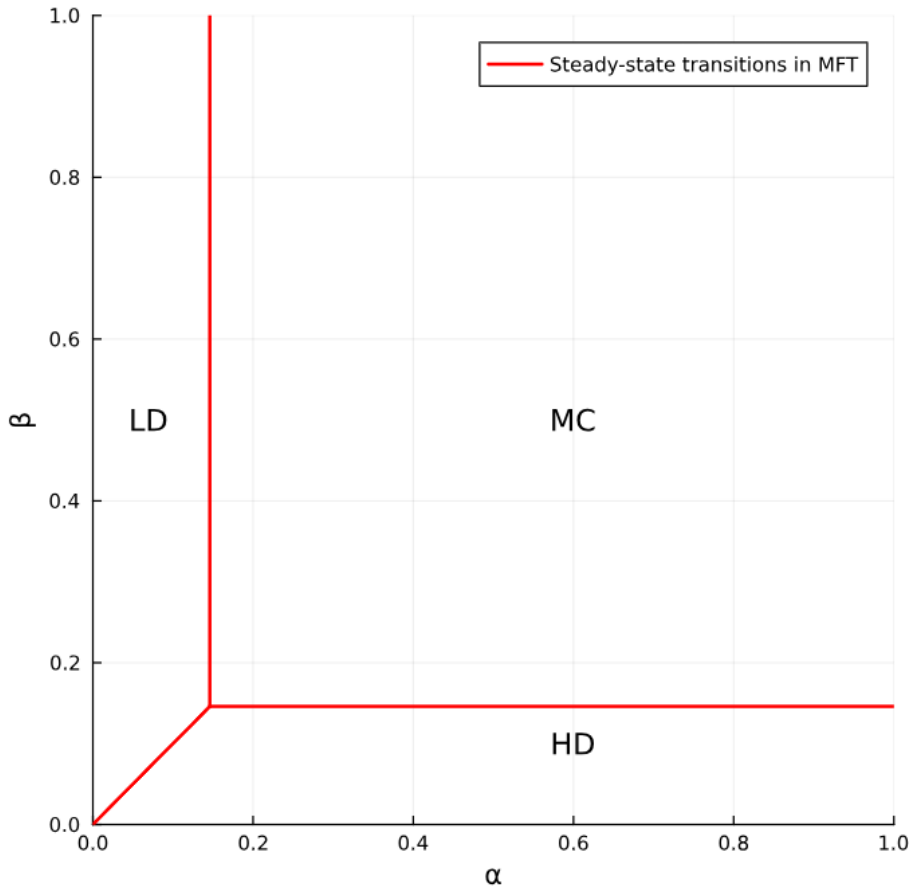

Figure 6: Phase diagram with steady-state transitions in MFT in the thermodynamic limit.

The steady-state density profile at the LD-HD transition is a Delocalized Domain Wall (DDW), whose position fluctuates along the lattice. Considering the bulk densities ρ_+ and ρ_-, the Domain Wall (DW) is a sharp interface that connects the two profiles (Fig. 7). We notice that, in presence of inhomogeneous hopping rates, the DW will spend different times at different positions. This means that the long time average of the density profile, i.e. the envelope of the DDW, is expected to be curvilinear, and not a straight line as in the homogeneous case (from now on we will call it envelope). We need to go beyond MFT to capture these fluctuations. Since the authors of [2] show that also the other two transitions (LD-MC and HD-MC) are first order, we expect to find a DDW at these transitions (Subsections 3.1 and 4.1).

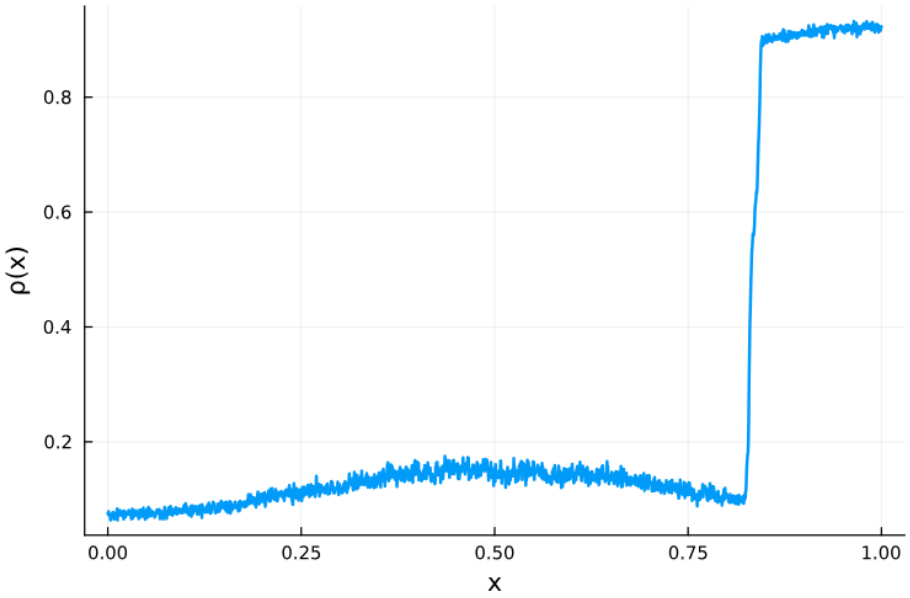

Figure 7: Short time average profile in MCS, obtained in the stationary state averaging in a short time frame ($5 \cdot 10^4$ time units): it is a Localized DW whose position randomly shifts with time.

3 Methods

Now we present the different methods used in order to deal with our tasks: FP equation, PA and MCS. The derivation of the MFT equations (discrete case) used for the numerical solutions can be found in Appendix A.

3.1 Fokker-Planck equation

One of the most important goals of this thesis is to find the density profiles at transitions. We first label the sites by $x = i/L$, with $i = 1, ..., L$. In the limit of $L \to \infty$, x becomes a continuous variable between 0 and 1. We work on LD-HD and LD-MC transitions. We do not need to consider the other one (HD-MC) due to the particle-hole symmetry of the model. Following [6], let x_w be the instantaneous position of the DDW and $\Delta(x_w)$ its height. Increasing the number of particles in the lattice by 1 will imply change the position x_w by an amount $\delta x_w = \frac{-1}{L\Delta}$. Clearly there are two processes which can alter the number of particles: particles entering from the left boundary and particles leaving the system on the right boundary.
Let $P(x_w, t)$ be the probability of finding a DW at x_w at time t. The currents at the left and right boundaries are:

$$J_{in} = \frac{1}{\tau(0)}\rho(0)(1-\rho(0)), \tag{19}$$

$$J_{out} = \frac{1}{\tau(1)}\rho(1)(1-\rho(1)). \tag{20}$$

Then, the average shift rate of the position is:

$$\langle \delta x_w \rangle = \frac{J_{out} - J_{in}}{L\Delta(x_w)}. \tag{21}$$

Since the DW performs a random walk around the mean position $\overline{x_w}$, for the condition $\langle \delta x_w \rangle = 0$ (fixed point of the random walk) we get:

$$J_{out} - J_{in} = 0. \tag{22}$$

Now we can write the master equation for the probability $P(x_w, t)$:

$$\frac{dP(x_w,t)}{dt} = \sum_{\delta x_w} \Big[P(x_w + \delta x_w, t) W(x_w + \delta x_w \to x_w) - P(x_w, t) W(x_w \to x_w + \delta x_w) \Big], \tag{23}$$

where $W(...)$ are the transition rates. We do not need to specify them because the hopping width is infinitesimal, so we can treat them in the FP approach.
We can now proceed with the Kramers-Moyal expansion [7] of the master equation (23) around $\overline{x_w}$ up to second order in δx_w, that is the FP equation:

$$\frac{dP(x_w,t)}{dt} = -\frac{\partial}{\partial x_w}[a(x_w)P(x_w,t)] + \frac{1}{2}\frac{\partial^2}{\partial x_w^2}[b(x_w)P(x_w,t)], \tag{24}$$

where:

$$a(x_w) = \sum_{\delta x_w} \delta x_w W(x_w + \delta x_w \to x_w), \tag{25}$$

$$b(x_w) = \sum_{\delta x_w} (\delta x_w)^2 W(x_w + \delta x_w \to x_w). \tag{26}$$

Using (22) we obtain:

$$a(x_w) = 0, \tag{27}$$

$$b(x_w) = \frac{1}{L^2 \Delta^2(x_w)} \left[\frac{1}{\tau(0)} \rho(0)(1-\rho(0)) + \frac{1}{\tau(1)} \rho(1)(1-\rho(1)) \right] > 0. \tag{28}$$

Finally we have (we can drop the subscript w):

$$\frac{dP(x,t)}{dt} = \frac{1}{2}\frac{\partial^2}{\partial x^2}[b(x)P(x,t)]. \tag{29}$$

In the steady state the left-hand side of (29) is equal to zero. Furthermore, since $J_{in} = J_{out}$, the DW obeys the detailed balance condition. It means that fluctuations in the DW position follow an equilibrium distribution. As a consequence, the probability current $J_{DW} = -\frac{1}{2}\frac{\partial}{\partial x}[b(x)P(x)]$ is zero, and we obtain:

$$P(x) = \frac{C}{b(x)}, \tag{30}$$

where the constant C can be calculated imposing normalization on $P(x)$.
The value of the envelope for a given coordinate x is:

$$\overline{\rho}(x) = \rho_-(x) Pr(x_w > x) + \rho_+(x) Pr(x_w < x). \tag{31}$$

The quantity:

$$\mathscr{P}(x) = \Pr(x_w < x) \tag{32}$$

is the cumulative distribution of x_w (denoting the random position of the DW), whose probability density is $P(x)$. Then, we can write:

$$\mathscr{P}(x) = \int_0^x P(x')\, dx'. \tag{33}$$

We also notice that:

$$\Pr(x_w > x) = 1 - \mathscr{P}(x). \tag{34}$$

Equation (31) can be rewritten:

$$\overline{\rho}(x) = \rho_-(x) + \Delta(x)\, \mathscr{P}(x), \tag{35}$$

where:

$$\Delta(x) \doteq \rho_+(x) - \rho_-(x) \tag{36}$$

is the height of the DW.

3.1.1 Low density-High density transition

According to the above discussion we have:

$$P(x) = \frac{C}{b(x)} \propto \Delta^2(x), \tag{37}$$

in which we have highlighted the dependence on the square of the height of the DW. At transition, where the current is $J = \frac{1}{\tau(0)}\alpha(1-\alpha)$, from equations (7), (8) and (36) we

have:

$$\Delta(x) = \sqrt{1 - 4\frac{\tau(x)}{\tau(0)}\alpha(1-\alpha)}. \tag{38}$$

For the probability density and the corresponding cumulative, from equations (33) and (37) we can write:

$$P(x) \propto Z + \cos(2\pi x), \tag{39}$$

$$\mathscr{P}(x) = \int_0^x P(x')\,dx' \propto Zx + \frac{1}{2\pi}\sin(2\pi x). \tag{40}$$

where $Z = \frac{1-6\alpha(1-\alpha)}{2\alpha(1-\alpha)}$. Imposing $\mathscr{P}(1) = 1$, we can determine the normalization constant. Then, taking into account (35) and (38) we finally get the envelope:

$$\overline{\rho}(x) = \sqrt{1 - 4\alpha(1-\alpha)\tau(x)}\left[x + \frac{\alpha(1-\alpha)}{1-6\alpha(1-\alpha)}\frac{\sin(2\pi x)}{\pi} - \frac{1}{2}\right] + \frac{1}{2}. \tag{41}$$

3.1.2 Low density-Maximal current transition

In this case, due to the behavior of the density profile at the transition, the DW will move only in the left half of the system, i.e. with $x \in [0, 1/2]$. Indeed, the LD profile coincides with the solution $\rho_-(x)$, whose behavior at LD-MC transition can be seen in Fig. 8, compared with the MC profile.
For $P(x)$ we have the same dependence as in the previous case. At the transition, where the current is $J = \frac{1}{4\tau_{max}}$, we find:

$$\Delta(x) = \frac{\cos(\pi x)}{\sqrt{2}}. \tag{42}$$

Following the same steps and imposing $\mathscr{P}(\frac{1}{2}) = 1$, the envelope becomes:

$$\overline{\rho}(x) = \frac{\cos(\pi x)}{\sqrt{2}}\left[2x + \frac{\sin(2\pi x)}{\pi} - \frac{1}{2}\right] + \frac{1}{2}. \tag{43}$$

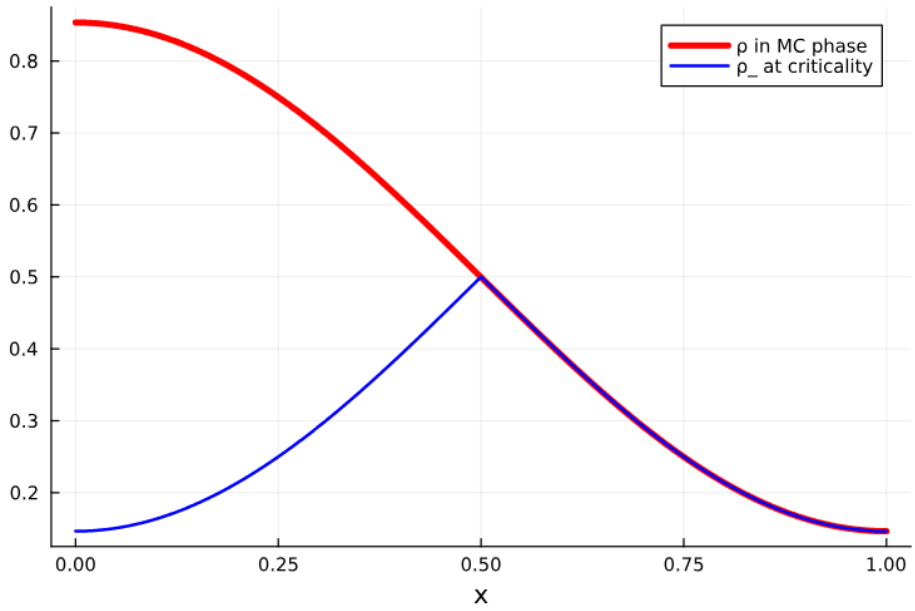

Figure 8: Density profile $\rho_{-}(x)$ at transition and MC profile.

3.2 Relaxation to the stationary state

In this subsection we want to discuss the relaxation toward the stationary state, and we will do it both at MFT and PA levels. Working in the inhomogeneous case, we will consider the inverse of (6) as the hopping rate function, but in the discrete scenario. So it is defined as q_i, for $i = 1, ..., L-1$.

3.2.1 Mean field theory

Linearizing the MFT equations for the time evolution of the local densities, close to the stationary state solution, we obtain:

$$\dot{\rho}_i^t = -\sum_{j=1}^{L} M_{ij}(\rho_j^t - \rho_j), \qquad i = 1, ..., L, \tag{44}$$

where ρ_j represents the stationary profile.
The matrix M characterizes relaxation. In particular, its smallest eigenvalue is the slowest relaxation rate, that is the inverse of the longest relaxation time. The numerical compu-

tation of its spectrum is particularly easy, since M is tridiagonal with elements:

$$M_{i,i} = -\left.\frac{\partial \dot{\rho}_i^t}{\partial \rho_i^t}\right|_{t\to\infty} = q_{i-1}\rho_{i-1} + q_i(1-\rho_{i+1}), \qquad i = 1, ..., L, \tag{45}$$

$$M_{i,i+1} = -\left.\frac{\partial \dot{\rho}_i^t}{\partial \rho_{i+1}^t}\right|_{t\to\infty} = -q_i\rho_i, \qquad i = 1, ..., L-1, \tag{46}$$

$$M_{i,i-1} = -\left.\frac{\partial \dot{\rho}_i^t}{\partial \rho_{i-1}^t}\right|_{t\to\infty} = -q_{i-1}(1-\rho_i), \qquad i = 2, ..., L. \tag{47}$$

Then, we can obtain the entries of M using Euler's method to solve the continuity equations describing the time evolution of the local densities.

3.2.2 Pair approximation

If we want to go beyond MFT, we need to take into account the evolution of the two-node marginals. Since the site occupation variables n_i^t ($i = 1, ..., L$) are binary, we can work with $n_i = n_{i+1} = 1$ as a reference. Considering the marginality relation between single-node and two-node probabilities:

$$P_i^t(1) = P_i^t(1,0) + P_i^t(1,1), \tag{48}$$

$$P_{i+1}^t(1) = P_i^t(0,1) + P_i^t(1,1), \tag{49}$$

and the fact that the single-node occupation probability coincides with the local density:

$$P_i^t(1) = \rho_i^t, \tag{50}$$

for the remaining two-node marginals (we do not need $P_i^t(0,0)$) one finds:

$$P_i^t(1,0) = \rho_i^t - P_i^t(1,1), \tag{51}$$

$$P_i^t(0,1) = \rho_{i+1}^t - P_i^t(1,1). \tag{52}$$

The evolution of the two-node marginal is dictated by:

$$\dot{P}_i^t(n_i, n_{i+1}) = \sum_{n\neq n_i, n_{i+1}} \sum_m \sum_{k=0}^{L} W_{n,m}^k P^t(m). \tag{53}$$

One can show (Appendix B) that:

$$\begin{aligned}
\dot{P}_i^t(1,1) &= q_{i-1}P_{i-1}^t(1,0,1) - q_{i+1}P_i^t(1,1,0), \qquad i = 2,...,L-2,\\
\dot{P}_i^t(1,1) &= \alpha P_i^t(0,1) - q_{i+1}P_i^t(1,1,0), \qquad i = 1,\\
\dot{P}_i^t(1,1) &= q_{i-1}P_{i-1}^t(1,0,1) - \beta P_i^t(1,1), \qquad i = L-1.
\end{aligned} \tag{54}$$

The PA assumes that correlations over three sites are negligible:

$$P_i^t(n_i, n_{i+1}, n_{i+2}) = \frac{P_i^t(n_i, n_{i+1})P_{i+1}^t(n_{i+1}, n_{i+2})}{P_{i+1}^t(n_{i+1})}, \tag{55}$$

where the denominator is needed to avoid counting the site $i+1$ twice. Taking into account the approximation (55), equation (54) becomes:

$$\begin{aligned}
\dot{P}_i^t(1,1) &= q_{i-1}\frac{P_{i-1}^t(1,0)P_i^t(0,1)}{P_i^t(0)} - q_{i+1}\frac{P_i^t(1,1)P_{i+1}^t(1,0)}{P_{i+1}^t(1)}, \qquad i = 2,...,L-2,\\
\dot{P}_i^t(1,1) &= \alpha P_i^t(0,1) - q_{i+1}\frac{P_i^t(1,1)P_{i+1}^t(1,0)}{P_{i+1}^t(1)}, \qquad i = 1,\\
\dot{P}_i^t(1,1) &= q_{i-1}\frac{P_{i-1}^t(1,0)P_i^t(0,1)}{P_i^t(0)} - \beta P_i^t(1,1), \qquad i = L-1.
\end{aligned} \tag{56}$$

Finally, defining $\phi_i^t \doteq P_i^t(1,1)$, equation (56) becomes:

$$\begin{aligned}
\dot{\phi}_i^t &= q_{i-1}\frac{(\rho_{i-1}^t - \phi_{i-1}^t)(\rho_{i+1}^t - \phi_i^t)}{1-\rho_i^t} - q_{i+1}\frac{\phi_i^t(\rho_{i+1}^t - \phi_{i+1}^t)}{\rho_{i+1}^t}, \qquad i = 2,...,L-2,\\
\dot{\phi}_1^t &= \alpha(\rho_2^t - \phi_1^t) - q_2\frac{\phi_1^t(\rho_2^t - \phi_2^t)}{\rho_2^t},\\
\dot{\phi}_{L-1}^t &= q_{L-2}\frac{(\rho_{L-2}^t - \phi_{L-2}^t)(\rho_L^t - \phi_{L-1}^t)}{1-\rho_{L-1}^t} - \beta\phi_{L-1}^t.
\end{aligned} \tag{57}$$

The evolution of the bulk local densities is described by the discrete continuity equation:

$$\begin{aligned}
\dot{\rho}_i^t &= q_{i-1}(\rho_{i-1}^t - \phi_{i-1}^t) - q_i(\rho_i^t - \phi_i^t), \qquad i = 2,...,L-1,\\
\dot{\rho}_1^t &= \alpha(1-\rho_1^t) - q_1(\rho_1^t - \phi_1^t),\\
\dot{\rho}_L^t &= q_{L-1}(\rho_{L-1}^t - \phi_{L-1}^t) - \beta\rho_L^t.
\end{aligned} \tag{58}$$

For the relaxation towards the stationary state we linearize equations (57) and (58), in order to find the relaxation matrix M (Appendix C).

3.3 Monte Carlo simulations

Over the course of this work we used both discrete and continuous time MCS.
We now delve deeper into the second one, using the Gillespie algorithm [8]. With this technique we randomly generate both the subsequent state of the system and the time at which the transition will happen. Analyzing systems in which states are discrete and the transition rate between two states n and m is $\mathscr{W}(n \to m)$, the probability for the system to leave the state n in an interval Δt is $\Delta t \sum_{b \neq n} \mathscr{W}(n \to b) \doteq \Delta t \ \mathscr{W}_n$. If we divide the interval $[0, t]$ into r subintervals of duration $\Delta t = t/r$, the probability that no state change occurs up to time t considering independent subintervals is:

$$P_r(t) = \left(1 - \Delta t \ \mathscr{W}_n\right)^r = \left(1 - \frac{t}{r} \ \mathscr{W}_n\right)^r \xrightarrow{\Delta t \to 0} \exp\left(-t \ \mathscr{W}_n\right). \tag{59}$$

Then, the probability that the system changes state at time t and not before is:

$$P_r(t) \ \mathscr{W}_n \xrightarrow{\Delta t \to 0} \ \mathscr{W}_n \exp\left(-t \ \mathscr{W}_n\right). \tag{60}$$

The algorithm works as follows:

1. generate two random numbers λ_1 and λ_2 from the uniform distribution U[0,1];

2. being at time t, the next transition will occur at time $t + \tau$, where:

$$\tau = -\frac{\ln(\lambda_1)}{\mathscr{W}_n}, \tag{61}$$

   comes from an exponential probability density;

3. being in state n, for each state m the probability to be selected is:

$$\frac{\mathscr{W}(n \to m)}{\mathscr{W}_n}; \tag{62}$$

the next state is chosen as follows:

$$\sum_{k=1}^{y-1} \mathscr{W}(n \to k) < \lambda_2 \ \mathscr{W}_n \leq \sum_{k=1}^{y} \mathscr{W}(n \to k); \tag{63}$$

4. update time and state.

4 Results

We can now discuss the results of this work, concerning both the stationary state and the relaxation towards it, comparing theoretical calculations and numerical solutions. Working on the envelope in the stationary state (Subsection 2.3), we used a criterion derived from the relaxation framework to strengthen the agreement between theoretical results and simulations; details will follow. An extra section will be dedicated to the full master equation, as a further study to better understand the effect of approximations.
We remark that in cases where we are studying a particular aspect of the model involving the MC phase and another one between LD and HD, we only need to consider one of the latter two, due to the particle-hole symmetry of the model.

Working in MFT and PA, for the solution of the differential equations involving single-node and two-node marginals we have considered Euler's method.
When we work in the thermodynamic limit, as we did in Subsection 3.1 in order to obtain the theoretical curve of the envelope or to find the theoretical value of the smallest eigenvalue of the relaxation matrix, we assume there is an infinite number of sites. Clearly, we cannot reproduce this feature in numerical MFT and MCS, so the idea is to use large values of L to reduce finite-size effects. For some results we show explicitly that these effects are reduced upon increasing the size of the system.
Since we start our simulations with an empty lattice we need to estimate the time beyond which we can start to sample the stationary state. This is done by considering a visual inspection of the evolution of the number of particles on the lattice. After the identification of an instant beyond which the number of particles seems stable, we choose a time T_0 ten times longer.
The final time T is obtained from a stop test applied to the derivative of the densities (threshold value).
Details about the number of sites L and the time values T and T_0 that we used can be found in the following sections.

4.1 Stationary state

As previously mentioned, one of the main goals of this thesis was to obtain the envelope at LD-HD and LD-MC steady-state transitions; let us also recall that we do not need to study

the HD-MC transition due to particle-hole symmetry. We compare the theoretical results of Subsection 3.1 with MCS. Since the location of the LD-HD transition is not affected by the finite size of the system, as it always occurs for $\alpha = \beta$ (due to symmetry reasons), we do not need a very large value of L. In Fig. 9 we can see a comparison between the theoretical envelope (red curve) and MCS with $L = 200$ (blue curve), for $\alpha = \beta = 0.05$; we used $T_0 = 10^6$; the final time is $T = 10^9$ ($\Delta = 0.01$ in Euler's method). In analogy with ordinary (homogeneous) TASEP, we expect that, averaging over relatively short time intervals, the profile exhibits two bulk regions separated by a DW, as previously shown in Fig. 7. In the limit of large L the DW can be anywhere, and the long-time average gives a profile that is almost linear, with a double slight curvature that is a sign of the inhomogeneous hopping rates (it is linear in the homogeneous case). We can see good agreement between the two curves.

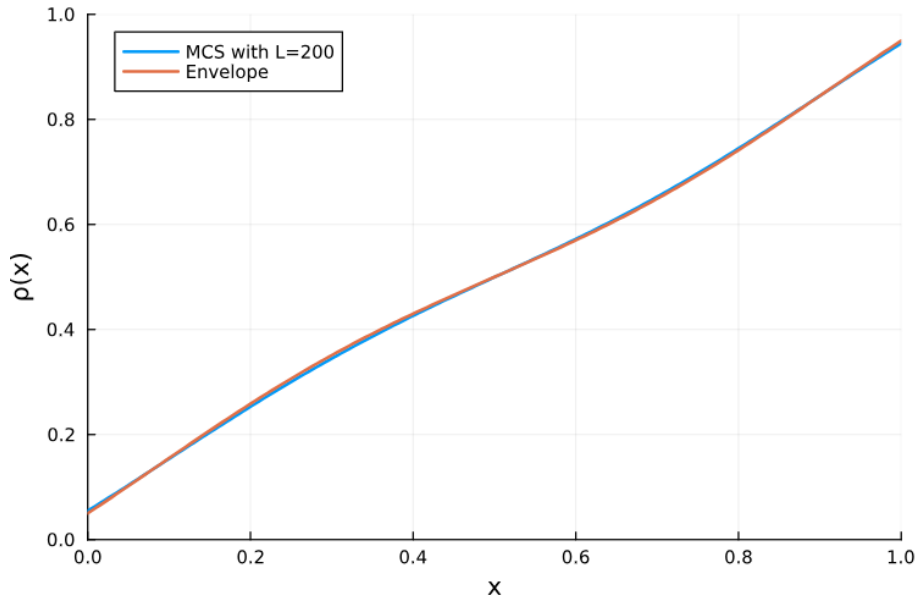

Figure 9: Envelope and MCS at the LD-HD transition (see the text).

The LD-MC transition is more difficult to investigate, due to the fact that finite-size effects influence the location of the transition line. Indeed, with a finite system we can only see a signature of the infinite size transition, and it is shifted to a greater value of α (β in the other one). In Fig. 10 we can see a comparison between the theoretical envelope and three MCSs with $L = 500$ and $\beta = 0.7$; $T_0 = 5 \cdot 10^5$; the final time is $T = 10^9$ ($\Delta = 0.01$ in Euler's method). As a support we also plot the bulk density

ρ_- at criticality and the MC profile (independent of α and β). We are working with $\alpha \in [0.1510, 0.1515]$ because within this interval, the density profiles show good agreement with the theoretical curve (Subsections 3.1). This can be connected with the relaxation matrix. Indeed, in the relaxation framework (Subsection 4.2) we calculate the smallest eigenvalue of the relaxation matrix, that is the inverse of the longest relaxation time of the system, and identify the range of the parameter for which the eigenvalue goes to zero. It corresponds to the phase transition (infinite relaxation time) and we can use that range as a criterion for selecting appropriate values of α to use in MCS. Due to finite-size effects there is no overlap between these two intervals, but they are really close to each other. We have also checked that, upon increasing L, this gap decreases.

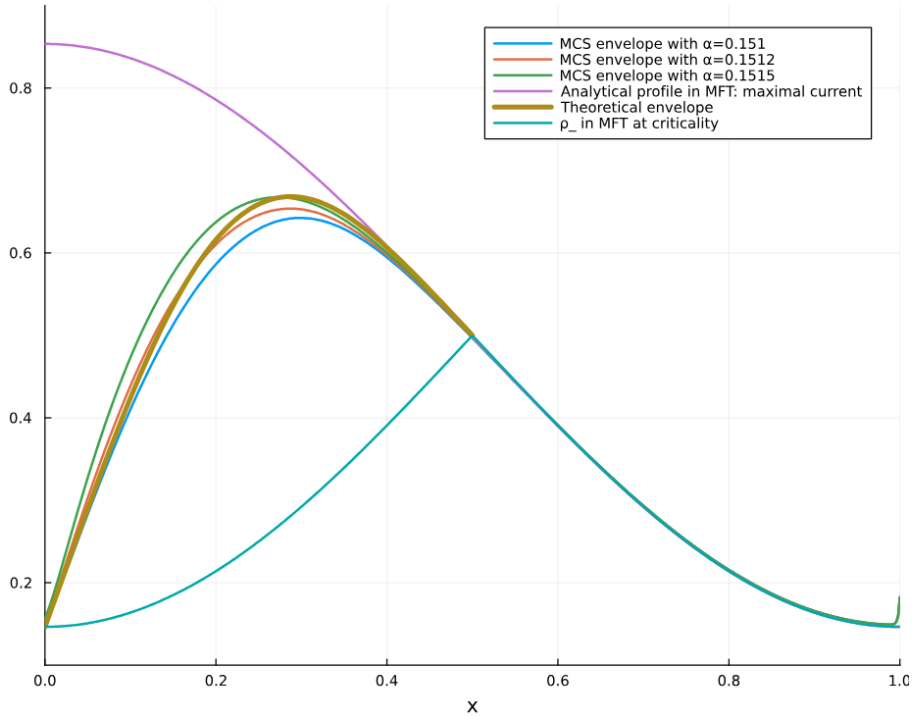

Figure 10: Envelope and MCS at the LD-MC transition (see the text).

Let us continue focusing on the LD-MC transition. Exploiting the property of the relaxation framework that we used before, it is also possible to show that, as the size L increases, the gap between the steady-state transitions at finite size and in the thermodynamic limit (both in MFT) decreases, at fixed parameters. The result is shown in Fig. 11.

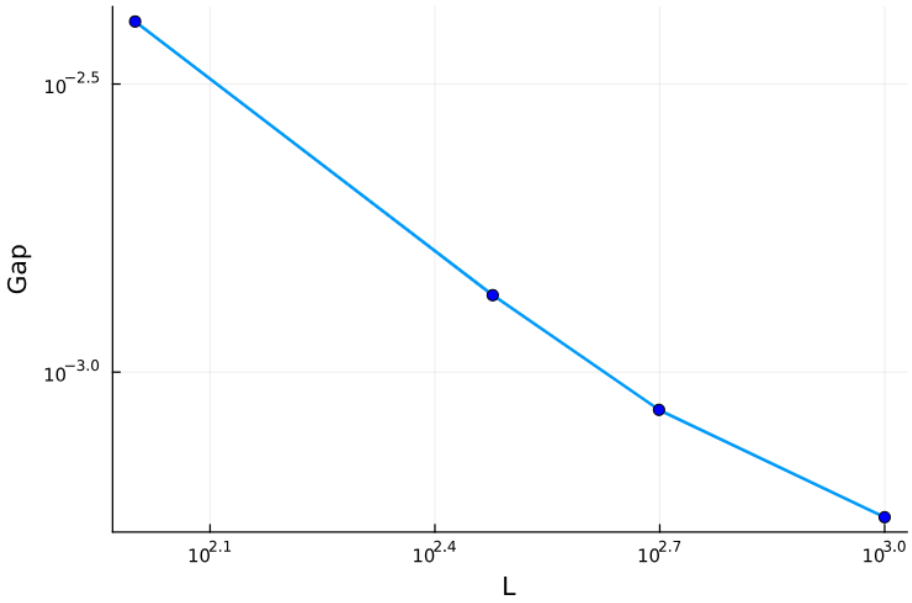

Figure 11: Log-Log plot of the gap between the steady-state transitions at finite size and in the thermodynamic limit, both in MFT, for $\beta = 0.5$.

Another interesting aspect of the stationary state is the scaling of the finite size density profiles. We have considered the MC phase. The goal is to show that when the data are correctly scaled, the finite size profiles collapse onto a universal curve, representing the asymptotic behavior in the thermodynamic limit. The main steps are: identification of the exponent γ of the power-law; rescaling $\frac{\Delta}{L^\gamma}$, where Δ is the gap between finite-size and thermodynamic profiles; comparison of the rescaled gaps for different values of L. An estimate of the exponent is $\gamma = -1$. The final result is plotted in Fig. 12 (only odd sites were considered for simplicity), for which we used $T = 2 \cdot 10^4$. We can see a really good agreement in the center of the lattice, while there is an increasing discrepancy moving towards the edges, due to the boundary layers.

4.2 Relaxation to the stationary state

In the context of the relaxation to the stationary state, the most interesting variable to study is the smallest eigenvalue of the relaxation matrix, that is the inverse of the longest relaxation time. We studied this regime with the MFT approach; then, we enrich the results using also PA (Subsection 3.2) and the full master equation.
Taking the HD phase as a reference, the main purpose was to detect the relaxation tran-

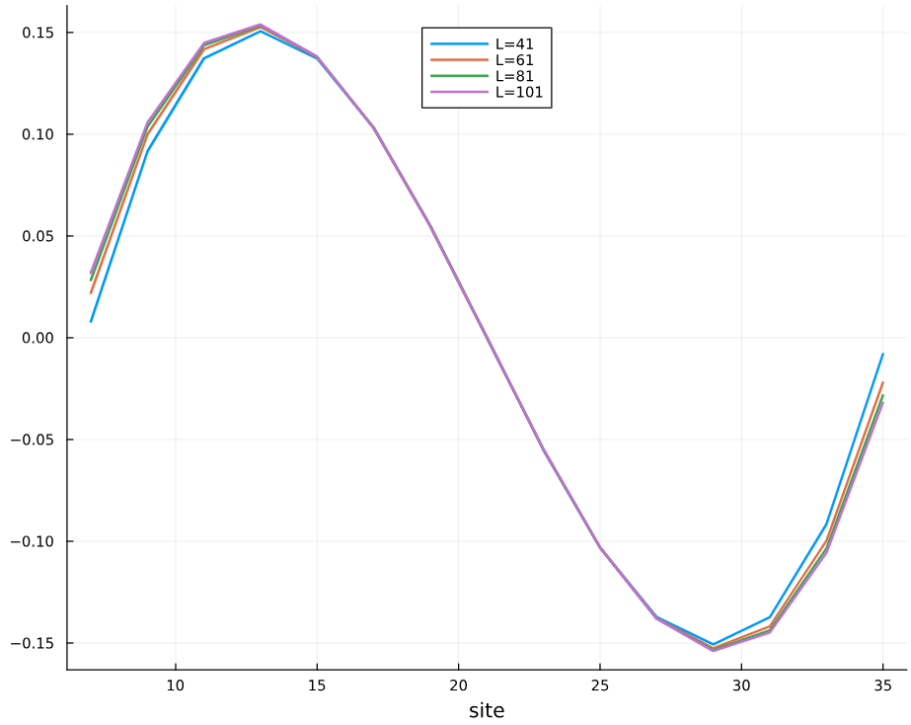

Figure 12: Scaling of the finite size density profile in MFT in the MC phase, considering the gap between the finite size profile and the one in the thermodynamic limit (see the text).

sition, represented by a critical curve $\alpha_c(\beta)$. For $\alpha > \alpha_c(\beta)$ the smallest eigenvalue is affected only by β, the parameter that determines the bulk density, while for $\alpha < \alpha_c(\beta)$ it becomes dependent also on α. Following [9, 10], it is possible to find the theoretical upper bound of the first eigenvalue in the thermodynamic limit, concerning the region with $\alpha > \alpha_c(\beta)$:

$$\lambda_1 = q_{min}\left(1 - \sqrt{\frac{4J}{q_{min}}}\right), \tag{64}$$

where $q_{min} = \frac{1}{\tau_{max}}$ is the minimum of the hopping rate function and J is the current. Also, it is possible to show that the theoretical approach can precisely predict the numerical MFT trend for $\alpha < \alpha_c(\beta)$ [10]. A comparison between numerical MFT and theoretical result can be seen in Fig. 13; for the numerical result we used $T = 2 \cdot 10^4$. Despite the discrepancy in the result, we find a good agreement for the region in which the eigenvalue

is α-independent; furthermore, this gap can be investigated and the trend is shown in Fig. 14 as a function of the size L, for $\beta = 0.09$ and $\alpha = 0.165$. We have checked the power-law behavior of this finite-size correction (Fig. 15).

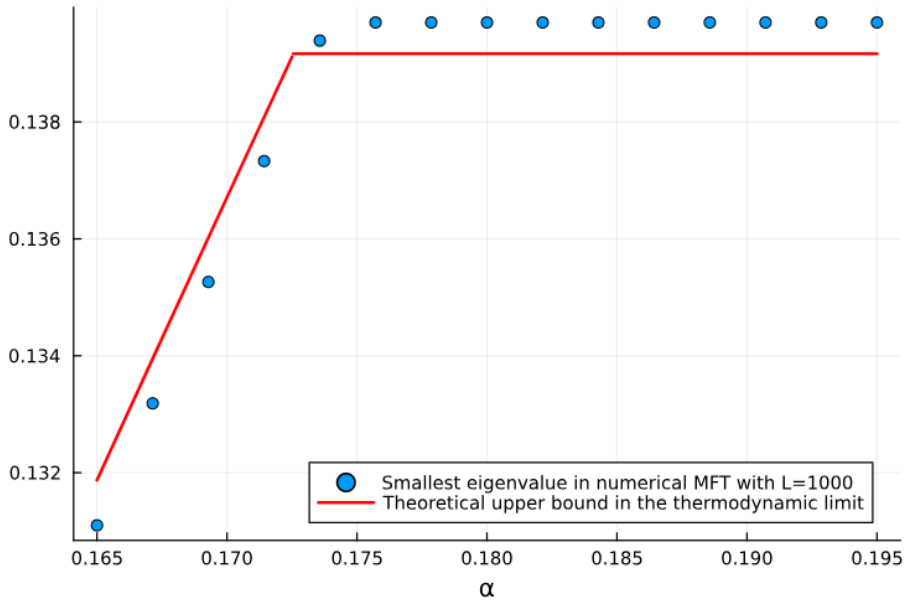

Figure 13: Comparison between the smallest eigenvalue in numerical MFT with $L = 1000$ and the theoretical upper bound in the thermodynamic limit, using $\beta = 0.07$.

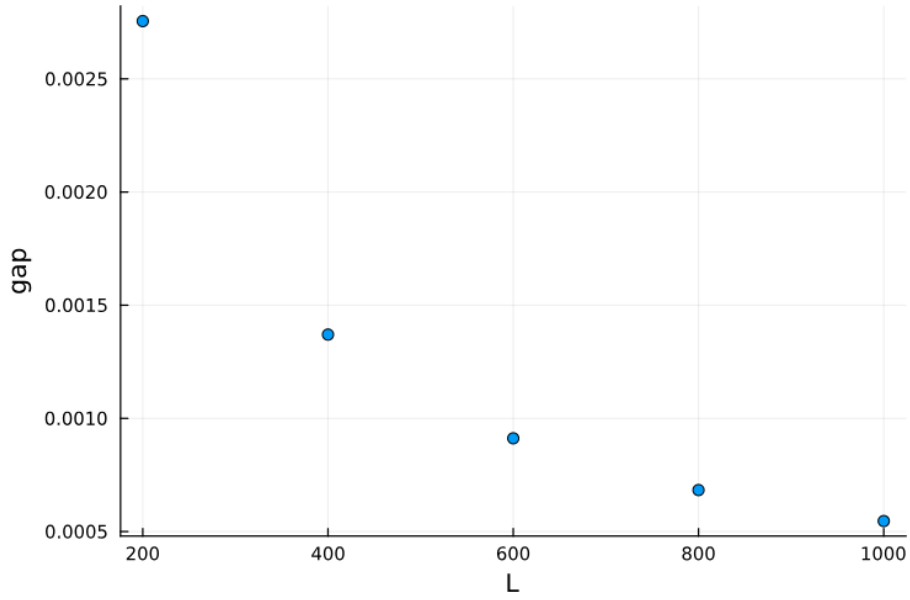

Figure 14: Gap between smallest eigenvalue in MFT and theoretical value, in the region with $\alpha > \alpha_c(\beta)$, for $\beta = 0.09$ and $\alpha = 0.165$.

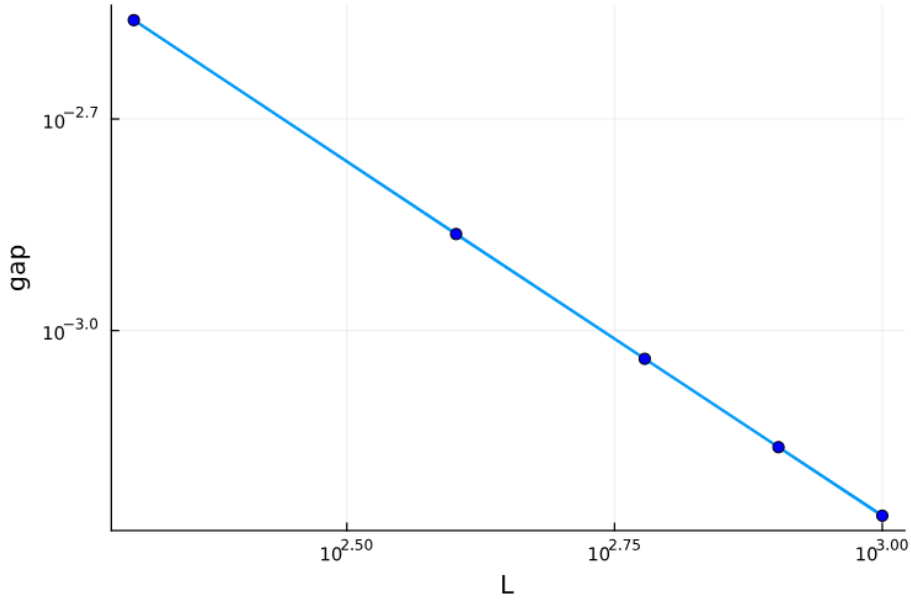

Figure 15: Log-Log plot of the gap between smallest eigenvalue in MFT and theoretical value, in the region with $\alpha > \alpha_c(\beta)$, for $\beta = 0.09$ and $\alpha = 0.165$.

Collecting data for different values of β, we were able to reconstruct the relaxation tran-

sition. The result is shown in Fig. 16, represented by the dots. Red lines represent the steady-state transitions, as obtained in Subsection 2.3. The phase diagram is truncated because the region with $\alpha, \beta > 0.7$ is not useful for the discussion.

A crucial element for the precise estimation of the transition points $\alpha_c(\beta)$ was the level crossing, a behavior for which the first eigenvalue sharply changes its slope, while a certain number of higher eigenvalues shows two subsequent slope changes, as we can see in Fig. 17. This behavior is not observed in the pure TASEP, but it appears in the TASEP with Langmuir Kinetics [10]. We used this crossing as a criterion to find the transition point, considering the intersection of two lines dictated by the trend of blue and green points, as we can see in the same figure (red lines). Thanks to this method, we avoid a more simplistic visual inspection.

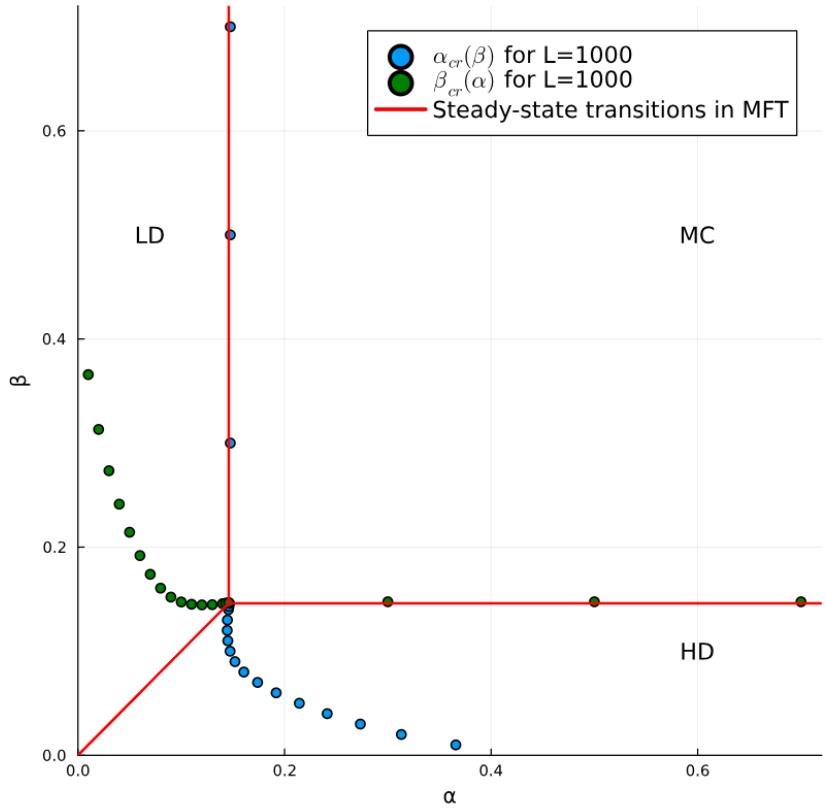

Figure 16: Phase diagram with steady-state and relaxation transitions.

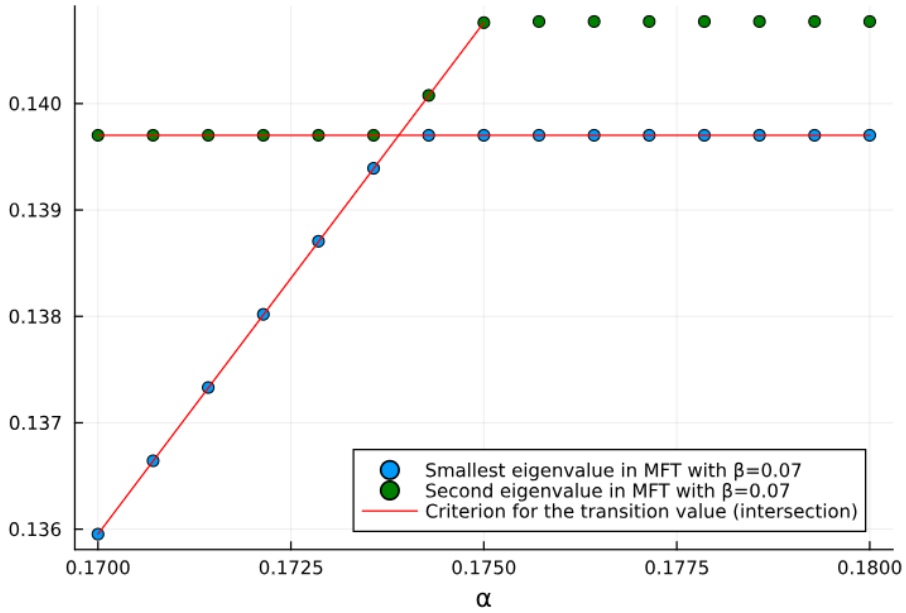

Figure 17: Level crossing in MFT.

In Fig. 16 we present the relaxation transitions highlighting that also approaching the MC phase from one of the other two, the smallest eigenvalue reaches a plateau (different from zero) and remains constant. But what we may expect is that this plateau goes to zero in the thermodynamic limit, as in the TASEP with homogeneous hopping rates. The numerical investigation can be seen in Fig. 18.
As we mentioned before, we can go beyond the MFT approximation and take into account at least nearest-neighbors correlations. We expect to find a greater relaxation time in PA, so a smaller eigenvalue, because within MFT we are considering the evolution of a smaller set of variables (reduced state space). A comparison between MFT and PA can be found in Fig. 19. We used $T = 2 \cdot 10^5$. Also in this case it is possible to show the presence of level crossing between eigenvalues.

Another relevant tool that we introduce in this section is the DWT [4]. It describes the dynamics of the system considering two different velocities, the shock velocity v_s and the group velocity v_g; we focus our efforts on the relaxation towards the stationary state, working with the shock velocity. We can consider the area included by 2 shock profiles at times t and $t + dt$, respectively at sites i and $i + 1$ (it is convenient to consider ρ_+ on the

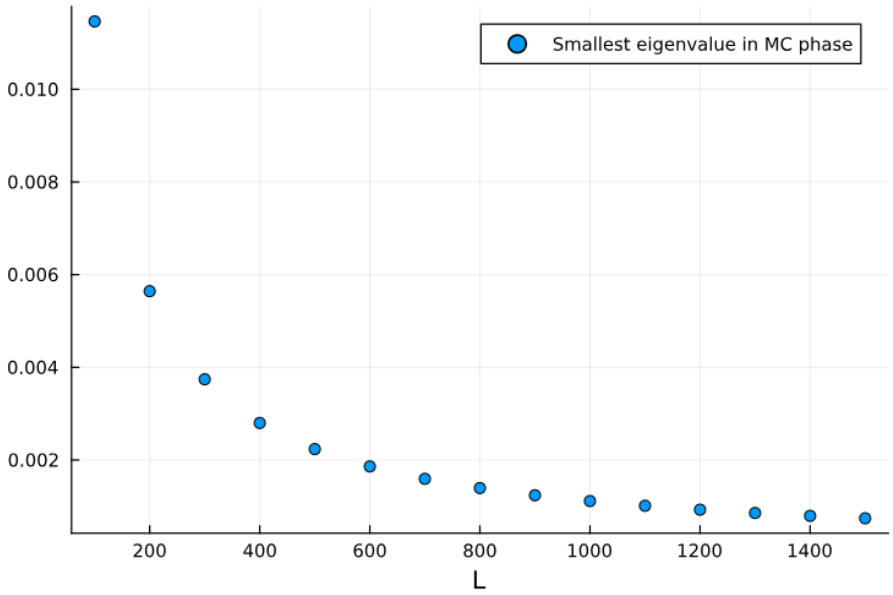

Figure 18: Smallest eigenvalue in MC phase for $\beta = 0.3$ and $\alpha = 0.16$.

right of the shock). This is approximately the area of a rectangle of height $\rho_+(i+1)-\rho_-(i)$ and width $v_s(i, i+1)dt$, but it also corresponds to a net number of particles:

$$J(q_{i+1}, \rho_+(i+1))dt - J(q_i, \rho_-(i))dt, \tag{65}$$

moving rightward in this time interval, where, due to the smoothness of the profile, $J(q_i, \rho(i)) = q_i\rho(i)[1-\rho(i)]$.
Then, the shock velocity is:

$$v_s(i, i+1) = \frac{J(q_{i+1}, \rho_+(i+1)) - J(q_i, \rho_-(i))}{\rho_+(i+1) - \rho_-(i)}. \tag{66}$$

The DWT main hypothesis is that the DW performs a biased random walk with hopping rates given by:

$$D_R(i) = \frac{J(q_i, \rho_+(i))}{\rho_+(i) - \rho_-(i-1)}, \qquad D_L(i) = \frac{J(q_i, \rho_-(i))}{\rho_+(i+1) - \rho_-(i)}. \tag{67}$$

Considering $P_n(t)$ as the probability that the DW is located at site n at time t, the master

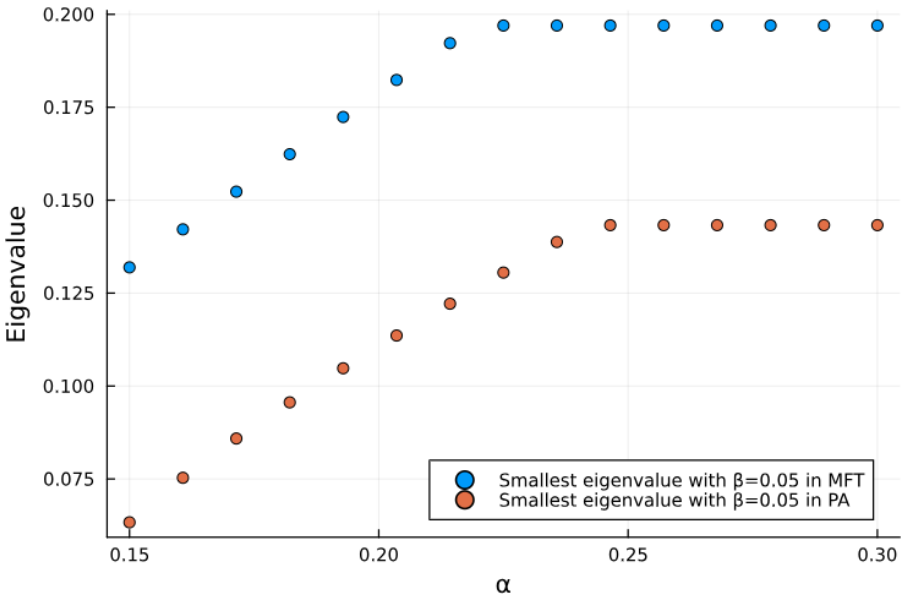

Figure 19: Smallest eigenvalue of the relaxation matrix: MFT and PA.

equation for its position is:

$$\begin{cases} \dot{P}_1(t) = -D_R(1)P_1(t) + D_L(2)P_2(t) \\ \dot{P}_n(t) = D_R(n-1)P_{n-1}(t) - [D_L(n) + D_R(n)]P_n(t) + D_L(n-1)P_{n+1}(t), \quad 1 < n < L \\ \dot{P}_L(t) = D_R(L-1)P_{L-1}(t) - D_L(L)P_L(t). \end{cases} \tag{68}$$

In matrix form we get:

$$\dot{P}(t) = -MP(t), \tag{69}$$

where the matrix M is tridiagonal; now we want to evaluate the smallest non-vanishing eigenvalue, i.e. the longest relaxation time of the system. We work in the HD phase. Since in the long-time limit the DW will be localized at the left boundary, and considering that the hopping rate function is cosinusoidal, i.e. smoothly varying, and assumes values close to 1 at the boundary, we expect that, for some range of α values, the smallest eigenvalue will be almost equal to that of the homogeneous case (where the hopping rates are constant and equal to 1). Since the boundary layer affects a small portion of the system, increasing

the size L it should become increasingly less relevant and lead to better agreement. Results can be shown in Fig. 20, for which we used $T = 10^5$. At the moment, we cannot give a clear interpretation of the plateau that is established from a certain value of α onwards, so further investigation will be necessary.

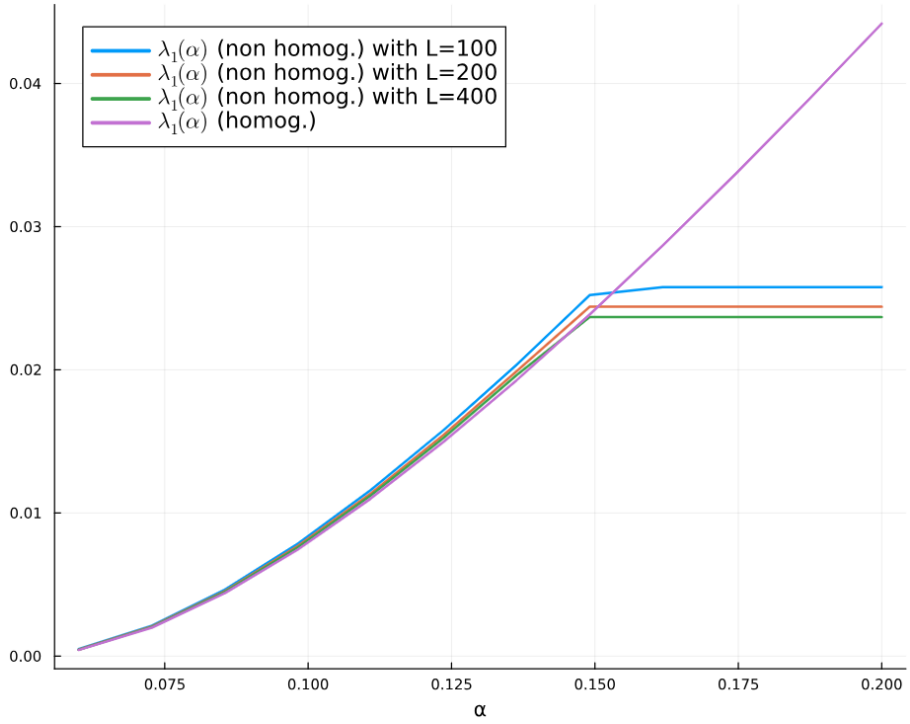

Figure 20: DWT: comparison between homogeneous and inhomogeneous cases in HD phase with $\beta = 0.05$.

4.3 Full master equation

Despite what we said in Subsection 2.2, we can try to study the full master equation for low values of L. Considering TASEP with OBC, transitions between different configurations can occur because of $L + 1$ possible processes, namely injection at node 1, hopping from node k to node $k + 1$ ($k = 1, ..., L - 1$) and extraction from node L. So, keeping in mind (1), we write:

$$W_{n,m} = \sum_{k=0}^{L} W_{n,m}^{k}. \tag{70}$$

Values $k = 1, ..., L-1$ describe hopping processes:

$$W^k_{n,m} = q_k \delta_{m_k,1} \delta_{m_{k+1},0} \left(\prod_{i \neq k,k+1} \delta_{n_i,m_i} \right) (n_{k+1} - n_k). \tag{71}$$

The value $k = 0$ describes the injection:

$$W^0_{n,m} = \alpha \delta_{m_1,0} \left(\prod_{i>1} \delta_{n_i,m_i} \right) (2n_1 - 1). \tag{72}$$

The value $k = L$ describes the extraction:

$$W^L_{n,m} = \beta \delta_{m_L,1} \left(\prod_{i<L} \delta_{n_i,m_i} \right) (1 - 2n_L). \tag{73}$$

Our first goal is to find the smallest non-vanishing eigenvalue of the transition rate matrix W. We expected to need a large enough value of L to see this eigenvalue reaching a plateau, and result is found in Fig. 21. It is possible to notice that, by increasing L, the plateau becomes more extensive. Moreover, for $L = 6$ we cannot really see a region in which the values become constant.

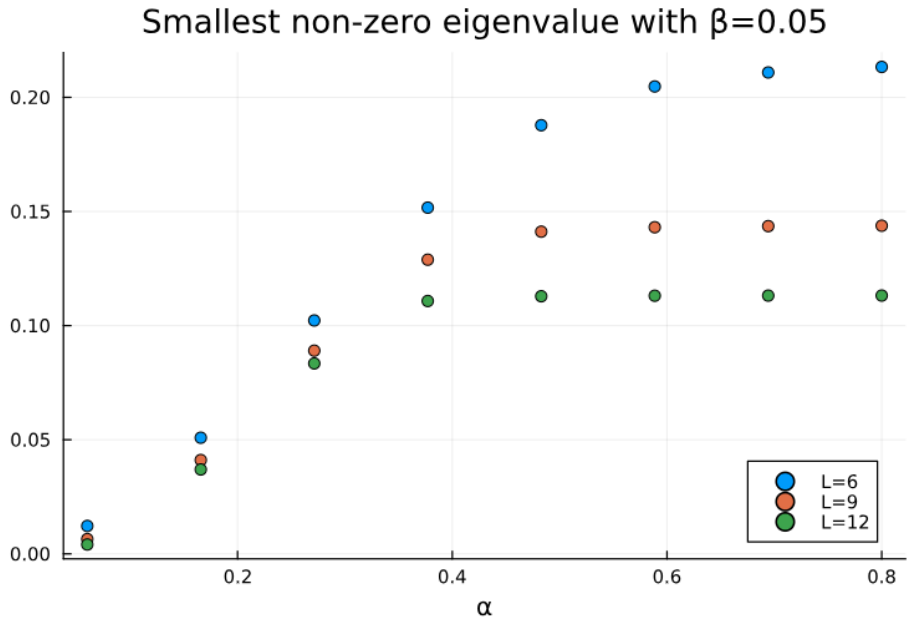

Figure 21: Smallest non-zero eigenvalue for three different values of the system size.

Then, one thing we can do is to compare this result with the one in PA. Since the PA takes into account only nearest-neighbour correlations, focusing on the plateau it is reasonable to find a smaller value of the eigenvalue in the full regime because the relaxation time is longer, due to higher-order correlations. The result can be seen in Fig. 22.

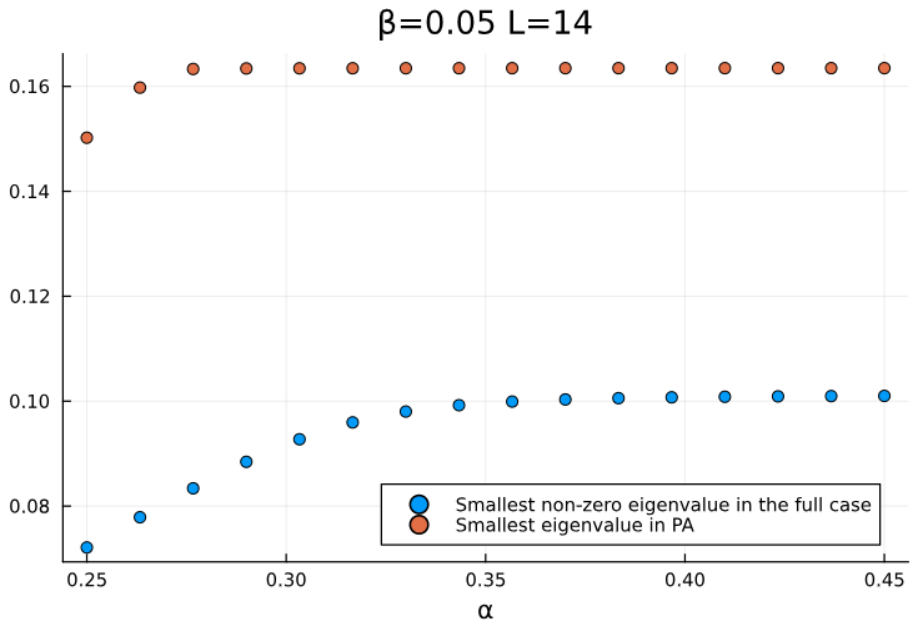

Figure 22: Comparison between smallest non-zero eigenvalues from full master equation and PA.

Finally, we are interested in the density profile that we can extrapolate from this discussion, that represents the exact finite-size profile. Result can be seen in Fig. 23, with a comparison with MFT and PA.

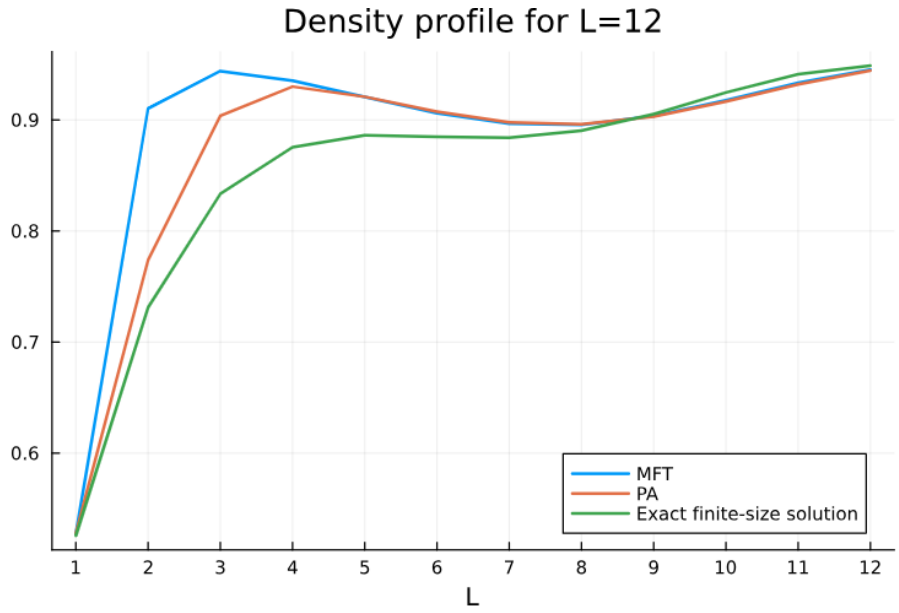

Figure 23: Comparison between exact finite-size solution, MFT and PA.

5 Conclusions

In this work we focused our efforts on the theoretical in-depth analysis of the TASEP with OBC and inhomogeneous hopping rates. We divide the problem into two main parts, the stationary state and the relaxation towards it.

For the stationary regime, we have considered the Fokker-Planck equation of the probability of the DW position. The theoretical envelope of the DDW at the transitions has been compared with MCS, showing a good agreement. In particular, the result we obtained for the LD-MC transition reinforces the idea that also at the LD-MC (and HD-MC) transition there is a DDW.

For the relaxation to the stationary state, we investigated the relaxation matrix using both MFT and PA approaches, to have a greater understanding of the problem. The phase diagram was obtained at the MFT level, showing both the steady-state and the relaxation transitions. The in-depth analysis regarding the finite size of the system shows that, increasing L, the gap between the smallest eigenvalue in MFT (size dependent) and the theoretical value (in the thermodynamic limit) decreases with power-law. Furthermore, the smallest eigenvalue in the MC phase seems to go to zero, increasing L. We enriched this study considering also the DWT.

Finally, we faced the full master equation for a system with low L. We checked that, increasing L, the behavior of the smallest non-zero eigenvalue shows the establishment of a plateau, as we seen in PA (or MFT) for a larger size of the system. Moreover, a comparison between the exact density profile and the one in PA (and MFT) shows that they become more and more similar, as we go away from the boundary layer.

6 Appendices

6.1 Appendix A

In this section we adopt the MFT approximation in the discrete case. Within this approximation we assume that at each instant t the joint probability factors into single-node marginals:

$$P_{MF}(n_1^t, ..., n_L^t) = p_1^t(n_1^t)p_2^t(n_2^t)....p_L^t(n_L^t). \tag{A1}$$

The local current is then given by:

$$J_i^t = q_i\rho_i^t(1-\rho_{i+1}^t), \qquad i = 1, ..., L-1, \tag{A2}$$

the continuity equation for the evolution of the local densities is:

$$\dot{\rho_i^t} = q_{i-1}\rho_{i-1}^t(1-\rho_i^t) - q_i\rho_i^t(1-\rho_{i+1}^t), \qquad i = 2, ..., L-1, \tag{A3}$$

with boundary conditions:

$$\begin{aligned}\dot{\rho_1^t} &= \alpha(1-\rho_1^t) - q_1\rho_1^t(1-\rho_2^t),\\ \dot{\rho_L^t} &= q_{L-1}\rho_{L-1}^t(1-\rho_L^t) - \beta\rho_L^t.\end{aligned} \tag{A4}$$

6.2 Appendix B

We consider:

$$\dot{P_l^t}(n_l, n_{l+1}) = \sum_{n\neq n_l, n_{l+1}} \sum_m \sum_{k=0}^{L} W_{n,m}^k P^t(m). \tag{B1}$$

We start from non-boundary nodes n_l $(l = 2, ..., L-2)$, working with $n_l = n_{l+1} = 1$. For $k = l-1$ we have:

$$\begin{aligned}\sum_{n\neq n_l, n_{l+1}} W_{n,m}^k &= q_{l-1}\delta_{m_k,1}\delta_{m_{k+1},0}\delta_{m_{l+1},n_{l+1}}\left(\prod_{i\neq k,k+1,k+2}\sum_{n_i}\delta_{n_i,m_i}\right)\sum_{n_k}^{1}(n_{k+1}-n_k)\\ &= q_{l-1}\delta_{m_k,1}\delta_{m_{k+1},0}\delta_{m_{l+1},1}.\end{aligned} \tag{B2}$$

$$\sum_{n\neq n_l,n_{l+1}}\sum_m W^k_{n,m}P^t(m) = q_{l-1}P^t_{l-1}(1,0,1). \tag{B3}$$

For $k = l$ we have:

$$\sum_{n\neq n_l,n_{l+1}} W^k_{n,m} = q_l\delta_{m_k,1}\delta_{m_{k+1},0}(n_{k+1}-n_k) = 0. \tag{B4}$$

$$\sum_{n\neq n_l,n_{l+1}}\sum_m W^k_{n,m}P^t(m) = 0. \tag{B5}$$

For $k = l+1$ we have:

$$\sum_{n\neq n_l,n_{l+1}} W^k_{n,m} = -q_{l+1}\delta_{m_k,1}\delta_{m_{k+1},0}\delta_{m_l,1}. \tag{B6}$$

$$\sum_{n\neq n_l,n_{l+1}}\sum_m W^k_{n,m}P^t(m) = -q_{l+1}P^t_l(1,1,0). \tag{B7}$$

All the other terms are zero. We get:

$$\dot{P}^t_l(1,1) = q_{l-1}P^t_{l-1}(1,0,1) - q_{l+1}P^t_l(1,1,0), \qquad l = 2,...,L-2. \tag{B8}$$

Now we consider the case with $l = 1$. For $k = 0$ we have:

$$\sum_{n\neq n_1,n_2} W^k_{n,m} = \alpha\delta_{m_1,0}\delta_{m_2,n_2}. \tag{B9}$$

$$\sum_{n\neq n_1,n_2}\sum_m W^k_{n,m}P^t(m) = \alpha P^t_1(0,1). \tag{B10}$$

For $k = 2$ we have:

$$\sum_{n\neq n_1,n_2} W^k_{n,m} = -q_2\delta_{m_k,1}\delta_{m_{k+1},0}\delta_{m_l,1}. \tag{B11}$$

$$\sum_{n\neq n_1,n_2}\sum_m W^k_{n,m}P^t(m) = -q_2P^t_1(1,1,0). \tag{B12}$$

Now we consider the case with $l = L-1$. For $k = L-2$ we have:

$$\sum_{n\neq n_{L-1},n_L} W^k_{n,m} = q_{L-2}\delta_{m_k,1}\delta_{m_{k+1},0}\delta_{m_{l+1},1}. \tag{B13}$$

$$\sum_{n\neq n_{L-1},n_L}\sum_m W^k_{n,m}P^t(m) = q_{L-2}P^t_{L-2}(1,0,1). \tag{B14}$$

For $k = L$ we have:

$$\sum_{n\neq n_{L-1},n_L} W^k_{n,m} = -\beta\delta_{m_L,1}\delta_{m_{L-1},n_{L-1}}. \tag{B15}$$

$$\sum_{n\neq n_1,n_2}\sum_m W^k_{n,m}P^t(m) = -\beta P^t_{L-1}(1,1). \tag{B16}$$

6.3 Appendix C

Linearizing equations (57) and (58) close to the stationary state solution, we get:

$$\dot{\rho}^t_i = -\sum_{j=1}^{L} M_{2i-1,2j-1}(\rho^t_j - \rho_j) - \sum_{j=1}^{L-1} M_{2i-1,2j}(\phi^t_j - \phi_j), \qquad i = 1,...,L. \tag{C1}$$

$$\dot{\phi}^t_i = -\sum_{j=1}^{L} M_{2i,2j-1}(\rho^t_j - \rho_j) - \sum_{j=1}^{L-1} M_{2i,2j}(\phi^t_j - \phi_j), \qquad i = 1,...,L-1. \tag{C2}$$

where the $(2L-1)\times(2L-1)$ matrix M is constructed in such a way that variables ρ and ϕ are written alternately (thus the non-zero elements are compacted around the diagonal). The entries of M are:

$$M_{2i-1,2i-1} = -\left.\frac{\partial\dot{\rho}^t_i}{\partial\rho^t_i}\right|_{t\to\infty} = q_i, \qquad i = 2,...,L-1, \tag{C3}$$

$$M_{1,1} = -\left.\frac{\partial\dot{\rho}^t_1}{\partial\rho^t_1}\right|_{t\to\infty} = \alpha + q_1, \tag{C4}$$

$$M_{2L-1,2L-1} = -\left.\frac{\partial\dot{\rho}^t_L}{\partial\rho^t_L}\right|_{t\to\infty} = \beta, \tag{C5}$$

$$M_{2i-1,2i+1} = -\left.\frac{\partial\dot{\rho}^t_i}{\partial\rho^t_{i+1}}\right|_{t\to\infty} = 0, \qquad i = 1,...,L-1, \tag{C6}$$

$$M_{2i-1,2i-3} = -\left.\frac{\partial\dot{\rho}^t_i}{\partial\rho^t_{i-1}}\right|_{t\to\infty} = -q_{i-1}, \qquad i = 2,...,L, \tag{C7}$$

$$M_{2i-1,2i} = -\left.\frac{\partial\dot{\rho}^t_i}{\partial\phi^t_i}\right|_{t\to\infty} = -q_i, \qquad i = 1,...,L-1, \tag{C8}$$

$$M_{2i-1,2i+2} = -\left.\frac{\partial\dot{\rho}^t_i}{\partial\phi^t_{i+1}}\right|_{t\to\infty} = 0, \qquad i = 1,...,L-2, \tag{C9}$$

$$M_{2i-1,2i-2} = -\left.\frac{\partial \dot{\rho}_i^t}{\partial \phi_{i-1}^t}\right|_{t\to\infty} = q_{i-1}, \qquad i = 2, ..., L, \tag{C10}$$

$$M_{2i,2i} = -\left.\frac{\partial \dot{\phi}_i^t}{\partial \phi_i^t}\right|_{t\to\infty} = -q_{i-1}\frac{\phi_{i-1}-\rho_{i-1}}{1-\rho_i} + q_{i+1}\frac{\rho_{i+1}-\phi_{i+1}}{\rho_{i+1}}, \qquad i = 2, ..., L-2, \tag{C11}$$

$$M_{2,2} = -\left.\frac{\partial \dot{\phi}_1^t}{\partial \phi_1^t}\right|_{t\to\infty} = \alpha + q_2\frac{\rho_2-\phi_2}{\rho_2}, \tag{C12}$$

$$M_{2L-2,2L-2} = -\left.\frac{\partial \dot{\phi}_{L-1}^t}{\partial \phi_{L-1}^t}\right|_{t\to\infty} = q_{L-2}\frac{\phi_{L-2}-\rho_{L-2}}{1-\rho_{L-1}} - \beta, \tag{C13}$$

$$M_{2i,2i+2} = -\left.\frac{\partial \dot{\phi}_i^t}{\partial \phi_{i+1}^t}\right|_{t\to\infty} = -q_{i+1}\frac{\phi_i}{\rho_{i+1}}, \qquad i = 1, ..., L-2, \tag{C14}$$

$$M_{2i,2i-2} = -\left.\frac{\partial \dot{\phi}_i^t}{\partial \phi_{i-1}^t}\right|_{t\to\infty} = -q_{i-1}\frac{\phi_i-\rho_{i+1}}{1-\rho_i}, \qquad i = 2, ..., L-1, \tag{C15}$$

$$M_{2i,2i-1} = -\left.\frac{\partial \dot{\phi}_i^t}{\partial \rho_i^t}\right|_{t\to\infty} = -q_{i-1}\frac{(\rho_{i-1}-\phi_{i-1})(\rho_{i+1}-\phi_i)}{(1-\rho_i)^2}, \qquad i = 2, ..., L-1, \tag{C16}$$

$$M_{2,1} = -\left.\frac{\partial \dot{\phi}_1^t}{\partial \rho_1^t}\right|_{t\to\infty} = 0, \tag{C17}$$

$$M_{2i,2i+1} = -\left.\frac{\partial \dot{\phi}_i^t}{\partial \rho_{i+1}^t}\right|_{t\to\infty} = -q_{i-1}\frac{\rho_{i-1}-\phi_{i-1}}{1-\rho_i} + q_{i+1}\frac{\phi_i}{\rho_{i+1}} - q_{i+1}\frac{\phi_i(\rho_{i+1}-\phi_{i+1})}{\rho_{i+1}^2}, \qquad i = 2, ..., L-2, \tag{C18}$$

$$M_{2,3} = -\left.\frac{\partial \dot{\phi}_1^t}{\partial \rho_2^t}\right|_{t\to\infty} = -\alpha + q_2\frac{\phi_1}{\rho_2} - q_2\frac{\phi_1(\rho_2-\phi_2)}{\rho_2^2}, \tag{C19}$$

$$M_{2L-2,2L-1} = -\left.\frac{\partial \dot{\phi}_{L-1}^t}{\partial \rho_L^t}\right|_{t\to\infty} = -q_{L-2}\frac{\rho_{L-2}-\phi_{L-2}}{1-\rho_{L-1}}, \tag{C20}$$

$$M_{2i,2i-3} = -\left.\frac{\partial \dot{\phi}_i^t}{\partial \rho_{i-1}^t}\right|_{t\to\infty} = -q_{i-1}\frac{\rho_{i+1}-\phi_i}{1-\rho_i}, \qquad i = 2, ..., L-2, \tag{C21}$$

$$M_{2L-2,2L-5} = -\left.\frac{\partial \dot{\phi}_{L-1}^t}{\partial \rho_{L-2}^t}\right|_{t\to\infty} = -q_{L-2}\frac{\rho_L-\phi_{L-1}}{1-\rho_{L-1}}. \tag{C22}$$

References

[1] Derrida B. and Evans M., Nonequilibrium Statistical Mechanics in One Dimension, Cambridge University Press (1997).

[2] Goswami A. et al., J. Stat. Mech. 123209 (2022).

[3] Stinchcombe R. B. and de Queiroz S. L. A., Phys. Rev. E 83 061113 (2011).

[4] Schadschneider A. et al., Stochastic Transport in Complex Systems, Elsevier, Amsterdam (2010).

[5] Hinsch H. et al., in Traffic and Granular Flow'05 (2007).

[6] Banerjee T. and Basu A., Phys. Rev. Res. 2 013025 (2020).

[7] Tauber U., Critical Dynamics, Cambridge University Press, Cambridge (2014).

[8] Gillespie D. T., J. Phys. Chem. 81 2340 (1977).

[9] Botto D. et al., J. Phys. A: Math. Theor. 52 045001 (2019).

[10] Botto D. et al., J. Phys. A: Math. Theor. 53 345001 (2020).